Neurobiology of Disease 127 (2019) 419–431

Contents lists available at ScienceDirect

Neurobiology of Disease

journal homepage: www.elsevier.com/locate/ynbdi

A mouse model for SPG48 reveals a block of autophagic flux upon disruption of adaptor protein complex five

Mukhran Khundadze[a,*], Federico Ribaudo[a], Adeela Hussain[a], Jan Rosentreter[a], Sandor Nietzsche[b], Melanie Thelen[c], Dominic Winter[c], Birgit Hoffmann[d], Muhammad Awais Afzal[a], Tanja Hermann[a], Cecilia de Heus[e], Eva-Maria Piskor[f], Christian Kosan[f], Patricia Franzka[a], Lisa von Kleist[g], Tobias Stauber[g], Judith Klumperman[e], Markus Damme[h], Tassula Proikas-Cezanne[i], Christian A. Hübner[a,*]

[a] Institute of Human Genetics, University Hospital Jena, Friedrich-Schiller-University Jena, Jena 07747, Germany
[b] Electron Microscopy Center, University Hospital Jena, Friedrich-Schiller-University Jena, Jena 07743, Germany
[c] Institute for Biochemistry and Molecular Biology, University of Bonn, Bonn 53115, Germany
[d] Biomolecular Photonics Group, University Hospital Jena, Friedrich-Schiller-University Jena, Jena 07743, Germany
[e] Department of Cell Biology, Center for Molecular Medicine, University Medical Center Utrecht, Utrecht 3584, Netherlands
[f] Institute of Biochemistry and Biophysics, Friedrich-Schiller-University Jena, Jena 07743, Germany
[g] Institute of Chemistry and Biochemistry, Freie Universität Berlin, Berlin 14195, Germany
[h] Institute of Biochemistry, Christian-Albrechts-University Kiel, Kiel 24118, Germany
[i] Department of Molecular Biology, Eberhard Karls University Tübingen, Tübingen 72076, Germany

ARTICLE INFO

Keywords:
AP5
ALR
Autophagy
Lysosome
SPG48

ABSTRACT

Hereditary spastic paraplegia is a spastic gait disorder that arises from degeneration of corticospinal axons. The subtype SPG48 is associated with mutations in the zeta subunit of the adaptor protein complex five (AP5). AP5 function and the pathophysiology of SPG48 are only poorly understood. Here, we report an AP5 zeta knockout mouse, which shows an age-dependent degeneration of corticospinal axons. Our analysis of knockout fibroblasts supports a trafficking defect from late endosomes to the *trans*Golgi network and reveals a structural defect of the Golgi. We further show that both autophagic flux and the recycling of lysosomes from autolysosomes were impaired in knockout cells. *In vivo*, we observe an increase of autophagosomes and autolysosomes and, at later stages, the accumulation of intracellular waste in neurons. Taken together, we propose that loss of AP5 function blocks autophagy and thus leads to the aberrant accumulation of autophagic cargo, which finally results in axon degeneration.

1. Introduction

Hereditary spastic paraplegia (HSP) is characterized as a progressive spastic gait disorder that arises from a length-dependent dying back degeneration of corticospinal tract fibers (Fink, 2014; Blackstone, 2018). More than 80 genetically distinct forms of HSP (SPGs) can be distinguished. SPG48 is transmitted as an autosomal recessive trait and is clinically highly variable with features such as sensory and motor neuropathy, ataxia, dystonia, myoclonus, and Parkinsonism in addition to spastic paraplegia. Because of the clinical overlap with lysosomal storage disorders and accumulation of multilamellar structures in patient derived skin fibroblasts, it was proposed that SPG48 may represent a new type of lysosomal storage disorder (Hirst et al., 2016).

Initially the gene mutated in SPG48 was identified in a screen for DNA double strand break repair. It encodes the protein KIAA0415, which co-precipitates in a complex with five other proteins (Slabicki et al., 2010), two of which being associated with HSP as well, *i.e.* Spatacsin mutated in SPG11 and Spastizin mutated in SPG15. Because of the difficulties to reliably detect the endogenous proteins, the functional interplay between KIAA0415, Spastizin and Spatacsin is still not fully resolved. It has been proposed that Spastizin and Spatacsin play a role in cell division (Sagona et al., 2010), autophagy (Vantaggiato et al.,

Abbreviations: AP, adaptor protein; ALR, autophagic lysosome reformation; HSP, hereditary spastic paraplegia; MEF, mouse embryonic fibroblast; SPG, spastic paraplegia gene; TGN, *trans*Golgi network

* Corresponding author at: Institute of Human Genetics, University Hospital Jena, Friedrich-Schiller-University Jena, Am Klinikum 1, Jena 07747, Germany.
E-mail addresses: Mukhran.Khundadze@med.uni-jena.de (M. Khundadze), Christian.Huebner@med.uni-jena.de (C.A. Hübner).

https://doi.org/10.1016/j.nbd.2019.03.026
Received 9 January 2019; Received in revised form 25 February 2019; Accepted 24 March 2019
Available online 28 March 2019
0969-9961/

2014), and endolysosomal trafficking (Hirst et al., 2013). Both proteins are involved in the recycling of lysosomes from autolysosomes (autophagic lysosome reformation) (Chang et al., 2014). This process is characterized by the formation of empty Lamp1-positive protrusions, which are finally pinched off from autolysosomes (Yu et al., 2010). Upon disruption of either Spastizin or Spatacsin, autophagosomes and autolysosomes increase in number, less of these autolysosomal tubules are formed and undegraded material accumulates over time (Khundadze et al., 2013; Vantaggiato et al., 2013; Chang et al., 2014; Varga et al., 2015).

Some years ago KIAA0415 and the other three proteins of the complex of unknown function were identified as the fifth adaptor protein complex because of the homology to other adaptor protein complexes with KIAA0415 being its zeta subunit (Hirst et al., 2011). Adaptor protein complexes are heterotetrameric protein complexes, which recognize and concentrate cargo proteins into vesicular carriers that mediate transport from a donor membrane to a target organelle. Although the cargo of AP5 is still largely unclear, elegant knockdown studies in HeLa cells suggest that AP5 is involved in the retrieval from the *trans*Golgi network to late endosomes (Hirst et al., 2018). Studies with patient iPSC-derived neurons from SPG48 patients further reported mitochondrial alterations (Denton et al., 2018).

Here, we describe a mouse model for SPG48, which is the first reported knockout mouse for a subunit of the AP5 complex. These mice accumulate autofluorescent material in neurons and develop late onset progressive gait abnormalities thus recapitulating the human phenotype. In agreement with a role of AP5 for the retrieval from late endosomes to the *trans*Golgi network, several Golgi-related proteins were enriched in lysosomal fractions of knockout mouse embryonic fibroblasts. Moreover, the Golgi apparatus was structurally altered. Analysis of autophagic flux and autophagic lysosome reformation upon starvation *in vitro* pointed to a defect of autophagic flux. This assumption was supported by the accumulation of autophagosomes and autolysosomes and the accumulation of undegraded autophagic cargo *in vivo*.

2. Materials and methods

2.1. Animals

Mice were housed with a 12 h light/dark cycle and fed on a regular diet *ad libitum*. All animal experiments were approved by the "Thüringer Landesamt für Lebensmittelsicherheit und Verbraucherschutz" (TLLV) in Germany (Approval number: 02-034-14).

The Ap5z1 knockout mouse strain used for this study was created from the embryonic stem cell clone EPD0587_5_A05 obtained from the KOMP Repository (www.komp.org) and generated by the Wellcome Trust Sanger Institute. Methods used on the CSD targeted alleles have been reported in (Skarnes et al., 2011). For genotyping DNA was isolated from tail biopsies. Genotyping primers were used in a single PCR reaction: f: GGAGCAA-CAGAACAAAGCTGTACG, KO-r: CGCCGGAACC GAAGTTCCTATTCC, WT-r: CAGGGCTGCTCACTCACCTACG. The primer pair f/WT-r amplified a 364 bp fragment for the wild-type allele and the primer pair f/KO-r a 250 bp fragment for the trapped allele. Experiments were conducted on mice with a mixed 129SVJ/C57BL/6 background.

2.2. Cell culture, mass spectrometry and immunoblot analyses

Mouse embryonic fibroblasts (MEFs) were prepared from E13.5 mouse pups and cultured in Dulbecco's Modified Eagle medium (DMEM) 1X with GlutaMAX-I supplemented with 10% FBS (Fetal Bovine Serum) and 1% penicillin/streptomycin (100×) in a humidified atmosphere with 5% CO_2 and 37 °C.

Hippocampal neurons were isolated from newborn pups and cultured as described previously (Sinning et al., 2011). Before transfection cells were plated on coverslips and after 24 h transfected with 1 µg DNA/well in 24-well plates with lipofectamine 3000 reagent (Invitrogen, Germany). 24 to 48 h post-transfection cells were fixed with 4% formaldehyde for 15 min at room temperature. Immunocytochemistry was performed as described (Sinning et al., 2011). The M6PR retrieval assay was performed as described in (Hirst et al., 2018). Images were acquired with a confocal scanning fluorescence microscope (Zeiss LSM 880, Germany) with Airyscan using a Plan-Apochromat 63×/1.4 oil DIC M27 objective and analyzed with the ZenBlue co-localization plugin (Zeiss, Germany). Quantitative measurements of the lysosomal proteome were carried out as described (Thelen et al., 2017). Protein enrichment analysis has been carried out by using of the cellular compartment tool from the Genome Ontology Consortium (GO) website (http://www.geneontology.org) (Ashburner et al., 2000; The Gene Ontology, 2017). Lysosomal pH measurements were performed as described previously (Weinert et al., 2010). For overexpression of the 103Q-HTT-GFP fusion protein, the variant cDNA was cut with *Kpn*I and *Xba*I from the pYES2/103Q plasmid of Michael Sherman (Addgene plasmid # 1385) (Meriin et al., 2002), and cloned into the pEGFP-N1 vector (Clontech laboratories, USA). To detect Zfyve26 and Spatacsin brain tissue was homogenized in a buffer containing 300 mM Tris-HCl pH 8.8, 5 mM EDTA, 3 mM NaF, 10% (*v*/v) glycerol, 3% (*w*/*v*) SDS, complete protease inhibitor cocktail (Roche, Switzerland) as described (Varga et al., 2015).

2.3. Time-lapse imaging for ALR

For detection of lysosomal tubules, MEFs were plated on 42 mm coverslips (PeCon, Germany) in 6 cm plates and transfected after 24 h with 3 µg of Lamp1-GFP plasmid DNA using Lipofectamine 3000 (Invitrogen, Germany). The Lamp1-GFP plasmid was a gift from Esteban Dell'Angelica (Addgene plasmid # 34831) (Falcon-Perez et al., 2005). To induce autophagy, cells were incubated with EBSS medium (Gibco, Germany) for 8–9 h. Tubulation events were visualized with a fluorescence microscope (CellObserver Z1, Zeiss, Germany) equipped with an incubation chamber (37 °C, 5% CO_2). Time-lapse images were acquired every 2 s for 3 min with an exposure time of 200 ms using the ApoTome mode and the 40×/1.2 W objective. Number and length of tubules were evaluated for 30 cells of each genotype in three independent experiments using ImageJ (National Institutes of Health, Bethesda, USA).

2.4. Histological analysis

Immunohistochemistry was done on formalin fixed, free floating sections as described previously (Sinning et al., 2011). Purkinje cell numbers were quantified on 40 µm sagittal brain sections after staining of brain sections with an antibody directed against Calbindin. For statistical analysis the number of Purkinje cells per 1,000 µm distance along the Purkinje cell layer was counted from three different cerebellar sections from three mice per genotype. Images of the sagittal sections of wild-type and knockout brains were taken with a confocal scanning fluorescence microscope (Zeiss LSM 880, Germany) with Airyscan using a Plan-Apochromat 63×/1.4 oil DIC M27 objective. Neurons were quantified with the cell counter plugin and the area measurement tool of ImageJ.

2.5. Ultrastructural analysis and morphometry

For semi- and ultrathin sectioning of brain samples, four animals per genotype were perfused with 50 ml fixative (4% formaldehyde, 2.5% glutaraldehyde in phosphate buffer). Brain and spinal cord were removed and post fixed overnight at 4 °C. 150 µm sagittal and coronal sections were cut with a vibratome (Leica Microsystems, Germany) and processed as described (Beetz et al., 2013).

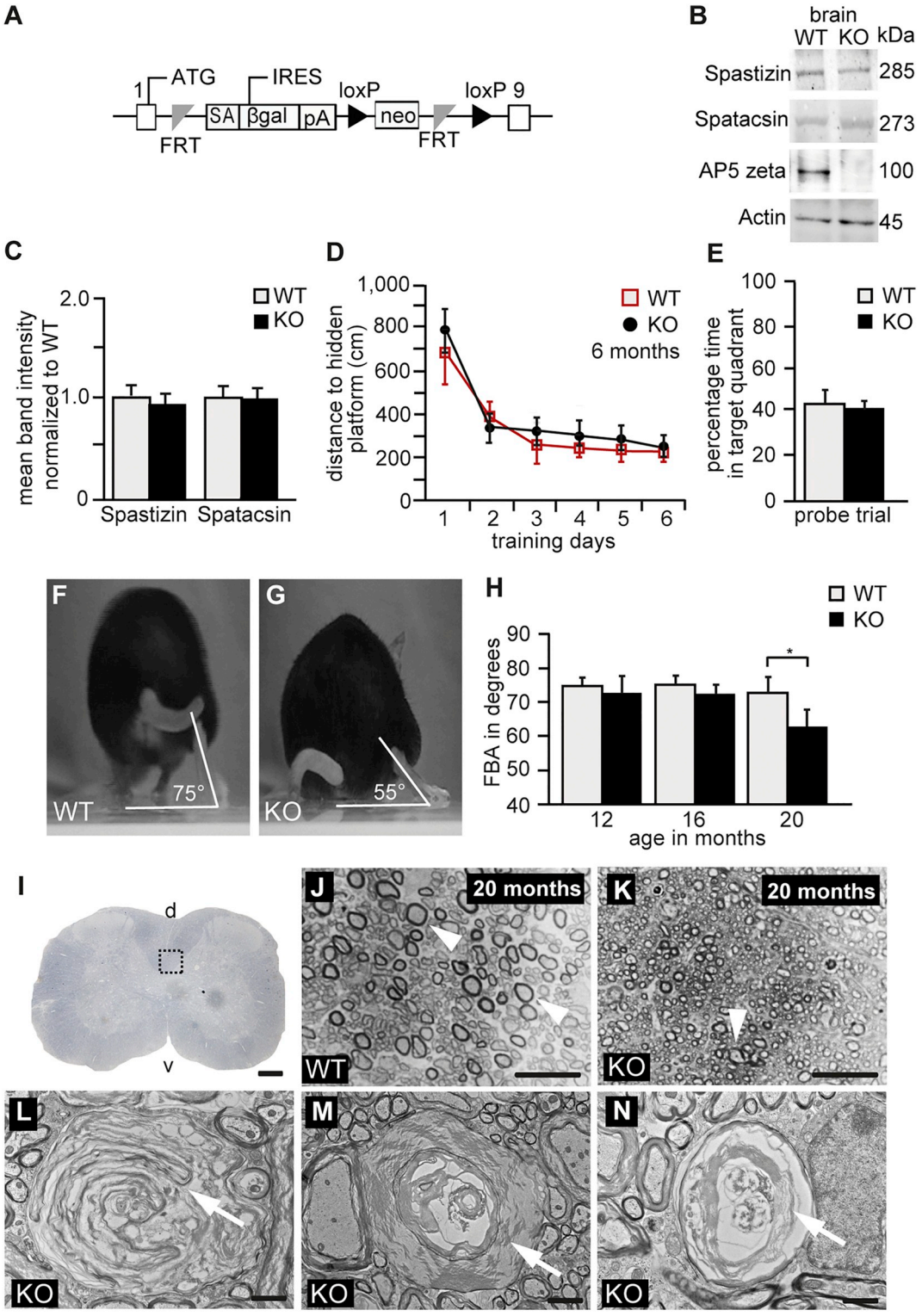

Fig. 1. Axon degeneration in AP5 zeta knockout mice. (A) Targeting strategy. Exons 2-8 of the *Ap5z1* gene are replaced by a gene trap cassette, which includes a splice acceptor (SA), internal ribosomal entry site (IRES), the β-galactosidase cassette (βgal) followed by a polyadenylation signal (pA) and a neomycin cassette (neo) flanked by loxP sites (black arrowheads). Both the βgal and neo cassette are flanked by frt sites (grey triangles). (B) Western Blot analysis of brain lysates with a polyclonal antibody directed against AP5 zeta detects a band of the predicted size in wild-type (WT) brain lysates, which is absent in homozygous trapped mice. Thus homozygous trapped mice represent AP5 zeta knockout mice (KO). Actin served as a loading control. (B,C) Spastizin and Spatacsin levels are not changed in total brain protein lysates of AP5 zeta KO mice (4 mice per genotype). (D-E) At six months of age no learning or memory deficits were noted in the Morris water maze (KO, $n = 8$; WT, $n = 7$; two-way ANOVA followed by Bonferroni test; $p > 0.05$). (F-G) Single video frames of a WT and a KO mouse walking on a beam at toe-off-position. The foot-base-angle (FBA) is indicated. (H) Compared to WT mice ($n = 9$) the FBA is decreased in 20 month-old AP5 zeta KO mice ($n = 10$) (two-way ANOVA followed by Bonferroni test; * $p < 0.05$). (I) Transversal semi-thin section of lumbar spinal cord to illustrate the regions shown in J and K. v: ventral; d: dorsal. Scale bar: 250 µm. (J, K) In comparison to controls large diameter axons (white arrowheads) are almost absent in the lumbar corticospinal tract of 20-month-old KO mice. Scale bars: 20 µm. (L-N) Transmission electron microscopy of lumbar corticospinal tract fibers illustrating different axonal pathologies including abnormal membranous material (white arrows) in AP5 zeta KO mice. Scale bars: 1.25 µm for L and N; 2.4 µm for M. Error bars in (C, D, E, H) represent mean ± SEM.

3. Results

3.1. Late onset corticospinal tract degeneration in AP5 zeta knockout mice

To generate AP5 deficient mice we injected the trapped embryonic stem cell clone EPD0587_5_A05 from the KOMP Repository (Fig. 1A) into donor blastocysts, which were transferred into foster mice. The resulting chimeric mice were mated to obtain heterozygous trapped mice. Mating of heterozygous offspring resulted in homozygous trapped mice at the expected Mendelian ratio. Validating that these represent AP5 zeta knockout mice, immunoblot analysis of brain lysates confirmed the absence of the AP5 zeta subunit (Fig. 1B). The abundance of Spatacsin and Spastizin, which are known to co-precipitate and interact with AP5 subunits (Slabicki et al., 2010; Hirst et al., 2011; Hirst et al., 2013), was not changed in brain lysates of AP5 zeta knockout mice (Fig. 1B, C).

Young knockout mice did not show any obvious abnormalities such as reduced body weight, motor deficits or increased mortality. In the Morris water maze paradigm the distance travelled to the hidden survival platform during the learning test (Fig. 1D) and the time spent in the target quadrant after removal of the survival platform in the memory test (Fig. 1E) did not differ between genotypes excluding a relevant spatial learning deficit at six months of age. To assess whether the AP5 zeta deficient mice develop a progressive gait abnormality we measured the foot base angle at toe-off position, when mice traversed a beam directing to the home cage as described previously (Beetz et al., 2013). In accordance with a rather mild motor phenotype in patients, we observed a significant flattening of this angle only at 20 months of age (Fig. 1F-H). At this time-point the morphological analysis of the lumbar corticospinal tract revealed a reduction of large diameter axons (Fig. 1I-K) and different signs of axon degeneration in knockout (Fig. 1L-N) but not in wild-type mice.

Taken together these findings are in agreement with late onset degeneration of the corticospinal tract, which results in a mild gait disturbance.

3.2. Accumulation of autofluorescent material in Purkinje neurons of AP5 zeta knockout mice

Starting around two months of age, neurons of different brain regions such as principal cells in the motor cortex and Purkinje cells accumulated autofluorescent deposits in both Spastizin and Spatacsin knockout mice (Khundadze et al., 2013; Varga et al., 2015). Although at a later time-point, an increase of autofluorescent material (emission wavelength 460–630 nm) was also evident in pyramidal neurons of layer V of the motor cortex (Fig. 2A, B) and in Purkinje neurons (Fig. 2E, F) in AP5 zeta knockout mice at eight months of age. At 20 months of age, only few dispersed and small autofluorescent spots were noted in wild-type mice (Fig. 2C, G), while larger clusters of autofluorescent material were a frequent finding in knockout mice (Fig. 2D, H). By ultrastructural analysis we observed larger clusters of membrane-associated electron-dense deposits of irregular shape in samples of aged knockout mice, which likely correspond with the autofluorescent material observed by light microscopy, but only some small particles resembling lipofuscin in aged control mice (Fig. 2I-J').

Because neurodegeneration frequently triggers the activation of astrocytes, we stained brain sections of 20-month-old mice for GFAP. Indeed, a strongly increased GFAP immunoreactivity was observed in knockout mice in different brain areas such as the Purkinje and granular cell layer of the cerebellum, while the molecular layer was spared (Fig. 2K, L). Labeling of Purkinje cells with Calbindin allowed us to quantify these cells. In contrast to Spastizin and Spatacsin knockout mice, where Purkinje cells were mostly lost at later stages, Purkinje cell bodies were preserved upon disruption of AP5 zeta (Fig. 2M).

In conclusion, morphological alterations in AP5 zeta knockout mice closely resemble findings in Spastizin and Spatacsin knockout mice but are less severe and occur later without overt Purkinje cell loss.

3.3. Accumulation of Lamp1-positive vesicles in axons of AP5 zeta knockout mice

It has been reported that AP5 localizes to the endolysosomal system (Hirst et al., 2013) and that SPG48 patient skin fibroblasts display abnormal endolysosomes (Hirst et al., 2015). To find an *in vivo* correlate in mice, we stained brain and spinal cord sections for the lysosomal membrane protein Lamp1. Notably, we found large Lamp1-positive spheroids with a diameter of up to 15 µm within the corticospinal tract of AP5 zeta knockout tissue, which were absent in control samples (Fig. 3A, B, B'). Electron microscopy suggested that these structures likely correspond with densely packed organelles such as mitochondria and vesicular structures (Fig. 3C) resembling lysosomes and autolysosomes (Fig. 3C′, C″). Similar Lamp1-positive structures were also found in the granular layer of the cerebellum (Fig. 3D). Because they co-labeled with Calbindin (Fig. 3D′, D″), which labels Purkinje cells, and the axonal marker protein Neurofilament 200 (Fig. 3E-E″), they likely represent swellings of Purkinje cell axons.

Taken together, clustering of organelles and Lamp1-positive vesicles underlies axonal swellings in AP5 zeta knockout mice.

3.4. Alterations of the transGolgi network in AP5 zeta knockout mouse embryonic fibroblasts

It has been reported that the morphology of mitochondria is changed in iPSC-derived neurons from SPG48 patients and upon knockdown of AP5 zeta in hEPCs (Denton et al., 2018). However, the morphology of Purkinje cell mitochondria at the ultrastructural level and the quantification of signal intensities for the mitochondrial marker protein Mtc02 in Purkinje cell bodies did not support gross changes of the mitochondrial pool in AP5 zeta knockout mice at 20 months of age (Fig. S1A-E).

We considered that AP5 may play a role for the sorting of lysosomal proteins. Therefore, we labeled control and AP5 zeta deficient mouse embryonic fibroblasts (MEFs) with either 'light' or 'heavy' isotope labeled-amino acids and isolated lysosomes with magnetic particles as reported previously (Thelen et al., 2017). Surprisingly, we did not find any striking alterations of typical lysosomal proteins, but rather an increase in several Golgi related proteins such as the Golgi glycoprotein one (Glg1) in the lysosomal fraction of knockout MEFs (Fig. 4A and Table S1), which is consistent with a defect in the trafficking between endolysosomea and Golgi.

To confirm that AP5 might act as a backup pathway for the retromer for the retrieval from late endosomes back to the Golgi apparatus (Hirst et al., 2018), we incubated MEFs from both genotypes with a M6PR antibody and chased the antibody for 60 min. Then cells were fixed and stained with a secondary antibody directed against the M6PR antibody and co-stained for TGN38 to label the *trans*Golgi network. In agreement with previous findings (Hirst et al., 2018), there was increased signal of the M6PR outside of the *trans*Golgi network area in AP5 zeta deficient MEFs (Fig. S2A-D). In addition, we noted a clear reduction of TGN38-signals in knockout MEFs, while the *cis*Golgi marker Giantin appeared unaltered (Fig. 4B-D). As judged from the ultrastructural analysis, there was an increase of cells with a more vesiculated Golgi apparatus and a significant decrease of the size of Golgi stacks in AP5 zeta knockout MEFs (Fig. 4E-H).

To get an idea whether these changes also apply *in vivo*, we stained sections of the cerebellum of two- and 20-month-old mice and quantified the TGN38- and Glg1-signals of individual Purkinje cell bodies. Interestingly, the TGN38- and Glg1-labeling did not differ between genotypes at two months, but was clearly reduced in AP5 zeta knockout mice at 20 months of age (Fig. 4I-Q). A decrease of Glg1 levels in AP5 zeta knockout mice was also confirmed by immunoblot analysis of brain lysates from 20-month-old mice (Fig. 4R), while protein abundance did

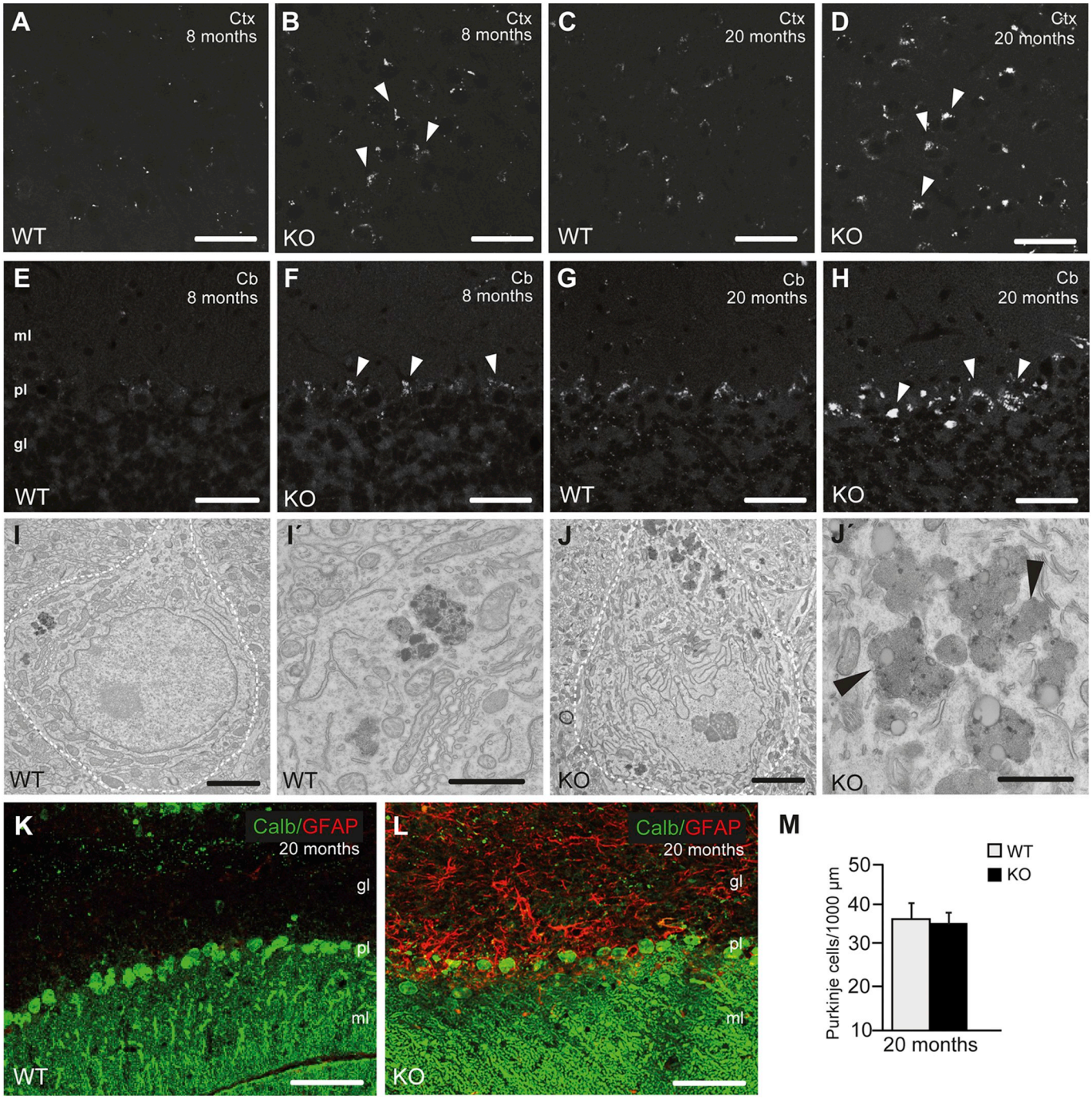

Fig. 2. Accumulation of autofluorescent material in AP5 zeta knockout neurons. (A-H) A substantial age-dependent increase of autofluorescent material was observed in pyramidal neurons in layer V of the motor cortex (A-D) and in Purkinje neurons (*E*-H) of knockout (B, D, F, H) compared to control mice (A, C, E, G) (excited at 488 nm, shown in white). Ctx: cortex; Cb: cerebellum; ml: molecular layer; pl: Purkinje cell layer; gl: granule cell layer. Scale bars: 50 µm. (I-J´) At the ultrastructural level electron dense material particles were more abundant in KO (J, J') compared to WT Purkinje cells (I, I′) at 20 months of age. The cell bodies of Purkinje cells are indicated by a dashed line. The magnification of the highlighted regions in (I) and (J) are shown in (I´) and (J´), respectively. Black arrowheads indicate membranes associated with the electron dense material. Scale bars: 2.5 µm for (I, J); 1.2 µm for (I′, J′). (K, L) Co-stainings for GFAP and Calbindin, which labels Purkinje cells, show a strong activation of astrocytes in the granular and Purkinje cell layer of KO mice at 20 months of age (L), while Purkinje cell bodies are preserved. Scale bars: 50 µm. (M) Quantification of Purkinje cells (three mice per genotype, Student's *t*-test; $p > 0.05$). Error bars represent mean ± SEM.

not differ at six months of age (Fig. S2E).

Thus, the disruption of AP5 zeta causes a redistribution of some Golgi related proteins to lysosomes and structural alterations of the Golgi apparatus in MEFs. Correlates of which were only detected in Purkinje neurons of aged knockout mice.

3.5. Impaired autophagy and autophagic lysosome reformation in AP5 zeta deficient MEFs

Western blot analysis did not reveal alterations of Lamp1 levels and the ratio between the mature and the precursor forms of the lysosomal protease Cathepsin D was unchanged in KO MEFs (Fig. 5A). Lysosomal

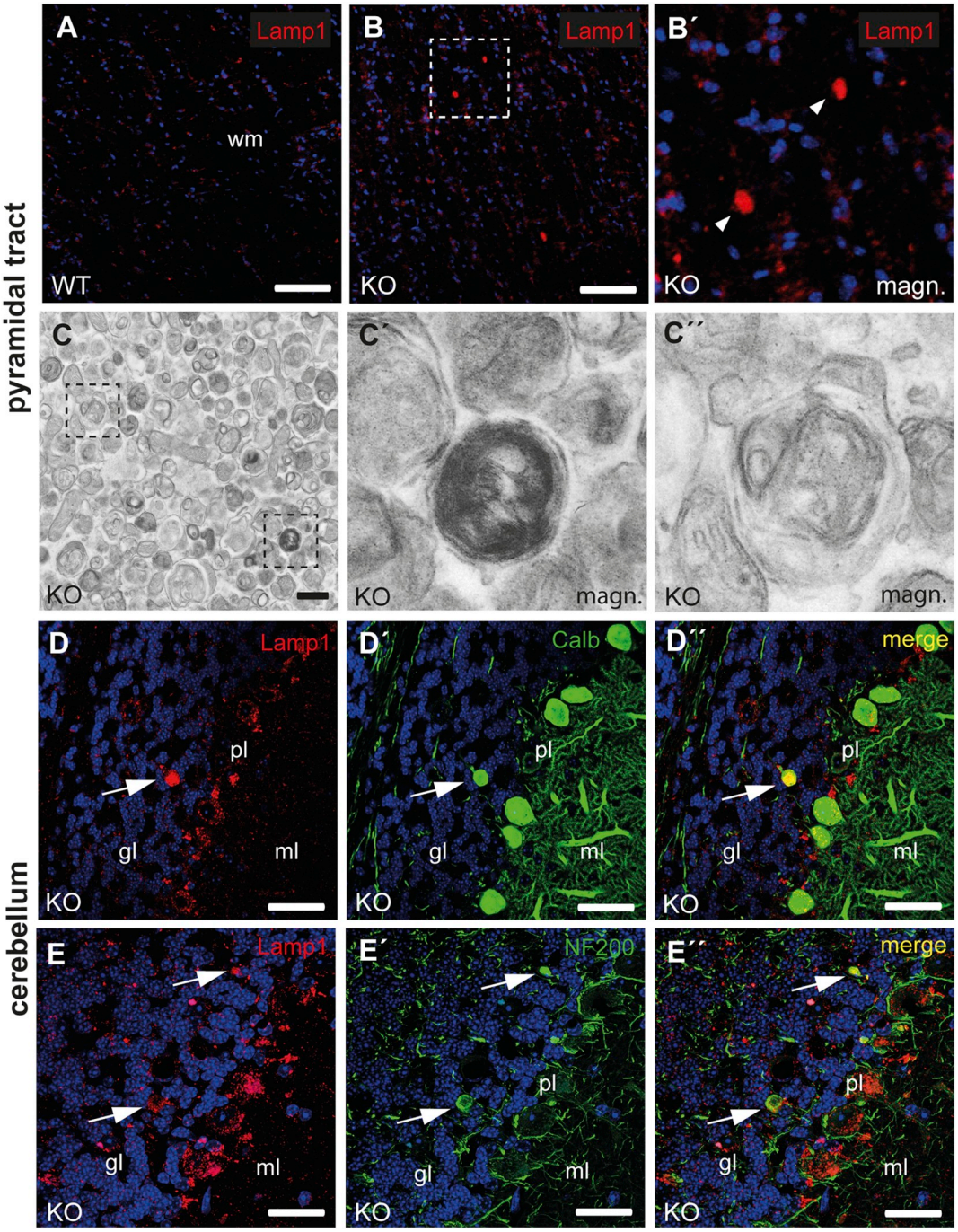

Fig. 3. Lamp1-positive axonal swellings in AP5 zeta knockout mice. (A-B′) At 20 months of age Lamp1-positive spheroids (Lamp1: red; blue: nuclei) are present in the corticospinal tract of the lumbar spinal cord of AP5 zeta KO mice (B) but not in controls (A). (B′) is a magnification of the region indicated in (B). Scale bars: 100 µm. (C-C″) The ultrastructural analysis identified clustered vesicles in some corticospinal tract axons (C). Magnifications of the regions indicated in (C) are consistent with lysosomes (C´) and autolysosomes (C″). Scale bar in C: 500 nm. (D-E″) Lamp1-positive spheroids are also detected in the cerebellar granule cell layer of 20-month-old KO mice (D, E), which also label for the Purkinje cell marker Calbindin (D′) and the axonal marker Neurofilament 200 (E′). The overlays are shown in (D″) and (E″). wm: white matter; pl: Purkinje cell layer, ml: molecular cell layer, gl: granule cell layer. Scale bars: 50 µm. (For interpretation of the references to colour in this figure legend, the reader is referred to the web version of this article.)

pH as an important determinant for the activity of lysosomal proteases also did not differ between genotypes (WT: 4.29, SE: ± 0.09; KO: 4.41, SE: ± 0.14) suggesting that the acidification of the lysosomal compartment is not compromised.

Further, we addressed whether autophagy may be impaired upon functional disruption of AP5 zeta. During the process of autophagy cytosolic LC3 (LC3-I) becomes conjugated to phosphatidylethanolamine at the nascent autophagosome, and is then referred to as LC3-II as it migrates faster in SDS-PAGE. Autophagosomes represent LC3-positive but Lamp1-negative double-membrane bound vesicles that sequester cytoplasmic material destined for degradation. Autophagosomes then fuse with lysosomes resulting in acidic Lamp1- and LC3-positive autolysosomes, in which the degradation of the engulfed material and LC3 by lysosomal enzymes takes place. Here, in basal autophagy conditions, both LC3-I and LC3-II abundances did not differ between genotypes (Fig. 5B, baseline). This result suggests that basal autophagy is not

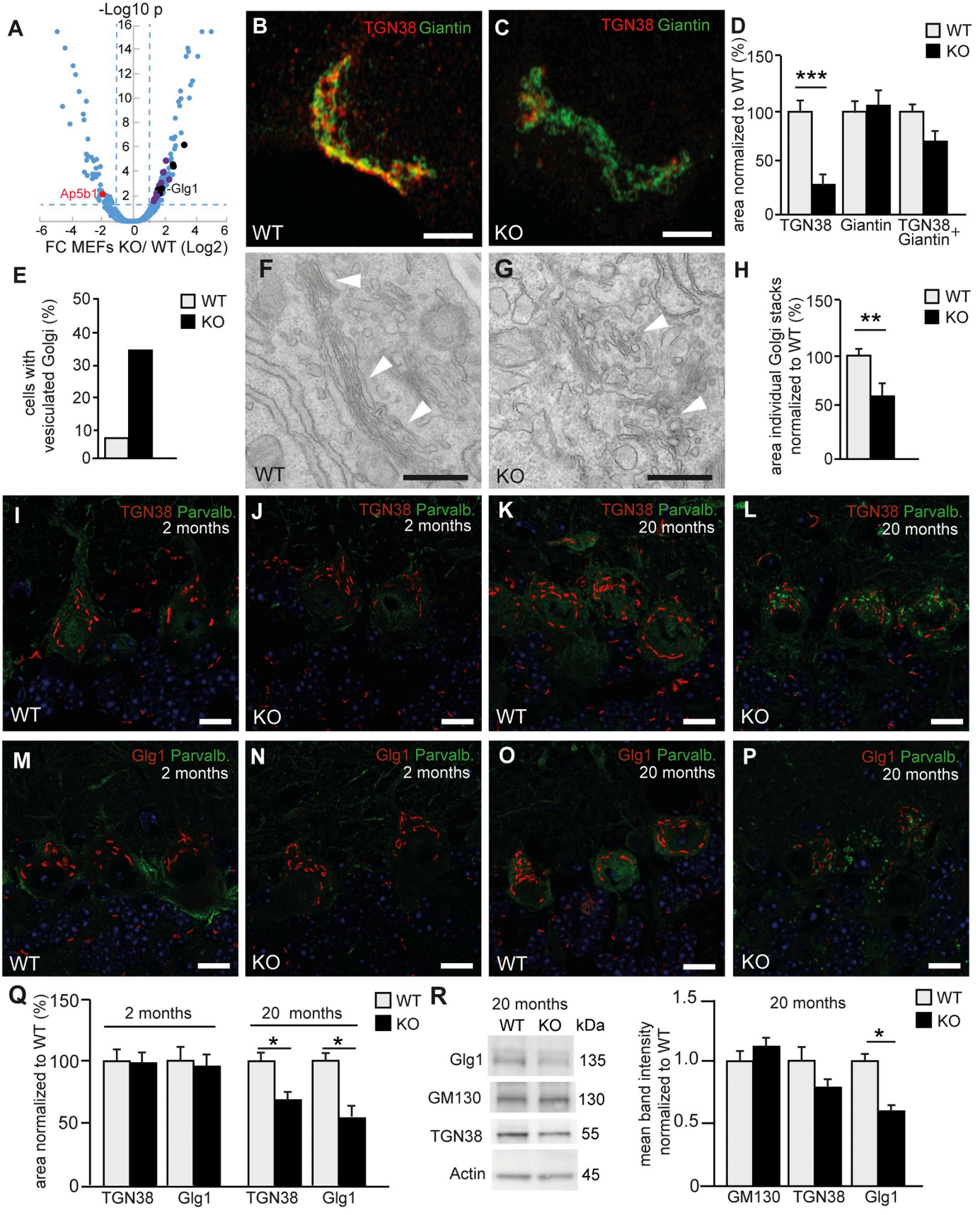

(caption on next page)

Fig. 4. Alterations of the Golgi apparatus upon disruption of AP5 zeta. (A) SILAC-based quantification of the proteome of lysosome enriched fractions from WT and KO mouse embryonic fibroblasts (MEFs) from four replica each. The complete list of differentially regulated proteins is shown in Table S1. The x-axis shows the log2-fold change (the fold change threshold > 1.0 is shown by blue dashed line) and the y-axis the respective -log10 *p*-value of significance analyzed by Student's *t*-test (significance threshold $p < 0.05$,). Differentially expressed endolysosome-associated proteins are shown as lilac colored dots; differentially expressed Golgi-associated proteins are shown as black colored dots. The spot representing the AP5 beta subunit is shown in red. (B-D) The relative area of TGN38-positive structures (*trans*Golgi) but not Giantin-positive structures (*cis*Golgi) are reduced in AP5 zeta KO MEFs. Scale bar: 1 µm. (E-H) The ultrastructural analysis of Golgi stacks revealed an increased number of MEFs with a vesiculated Golgi apparatus (E). Exemplary images are shown in (F) and (G). The Golgi complex is indicated by white arrowheads. (H) Overall the mean size of individual Golgi stacks was decreased. Student's *t*-test (40 cells per genotype; ** $p < 0.01$). Scale bars: 500 nm. (I-Q) Signals for the *trans*Golgi proteins TGN38 and Glg1 were reduced in Purkinje cells in brain sections of 20- but not two-month-old KO mice. Student's *t*-test (over 30 cells from three mice per genotype; * $p < 0.05$). Scale bars: 10 µm. (R) A reduction of Glg1 abundance was confirmed by immunoblot analysis of total brain lysates of 20-month-old mice. Actin served as a loading control. Student's *t*-test (three mice per genotype; * $p < 0.05$). Error bars in (D, H, Q, R) represent mean ± SEM. (For interpretation of the references to colour in this figure legend, the reader is referred to the web version of this article.)

affected in AP5 zeta KO MEFs. In contrast, under conditions were we induced autophagy by starvation with EBSS we observed that the abundance of LC3-II was significantly increased in AP5 zeta knockout MEFs (Fig. 5B, EBSS and EBSS + Torin1). However, when we starved the cells with EBSS while inhibiting lysosomal function by Bafilomycin A1 administration, we did not observe a significant increase of LC3-II in AP5 KO MEFs compared to WT (Fig. 5B, EBSS + BafA), suggesting a block in the autophagic flux in the absence of AP5. In order to challenge this assumption, we starved WT and AP5 zeta KO MEFs for 4 h and co-stained endogenous LC3 and Lamp1 to assess co-localizing LC3/Lamp1 puncta, indicative for autolysosomes (Fig. 5C-H). In line with our western blot results (Fig. 5B) we were unable to observe a difference in the numbers of autolysosomes (AL, LC3/LAMP1-positive yellow puncta) in basal autophagy conditions (Fig. 5C-E). Consistently, we also did not observe an increase of autophagosomes (AP, LC3-positive green puncta) and the numbers of lysosomes also did not change (Lys, Lamp1-positive red puncta) (Fig. 5C-E). However, upon starvation-induced autophagy (Fig. 5F-H), we detected a significant increase in the numbers of autophagosomes (AP, LC3, green puncta), as well as a significant decrease in the numbers of autolysosomes (AL, LC3/Lamp1, yellow puncta). Taken together, our results strongly indicate that in the absence of AP5 zeta the autophagic flux is blocked under stressed conditions, such as starvation.

Based on this observation we hypothesized that blocked autophagy

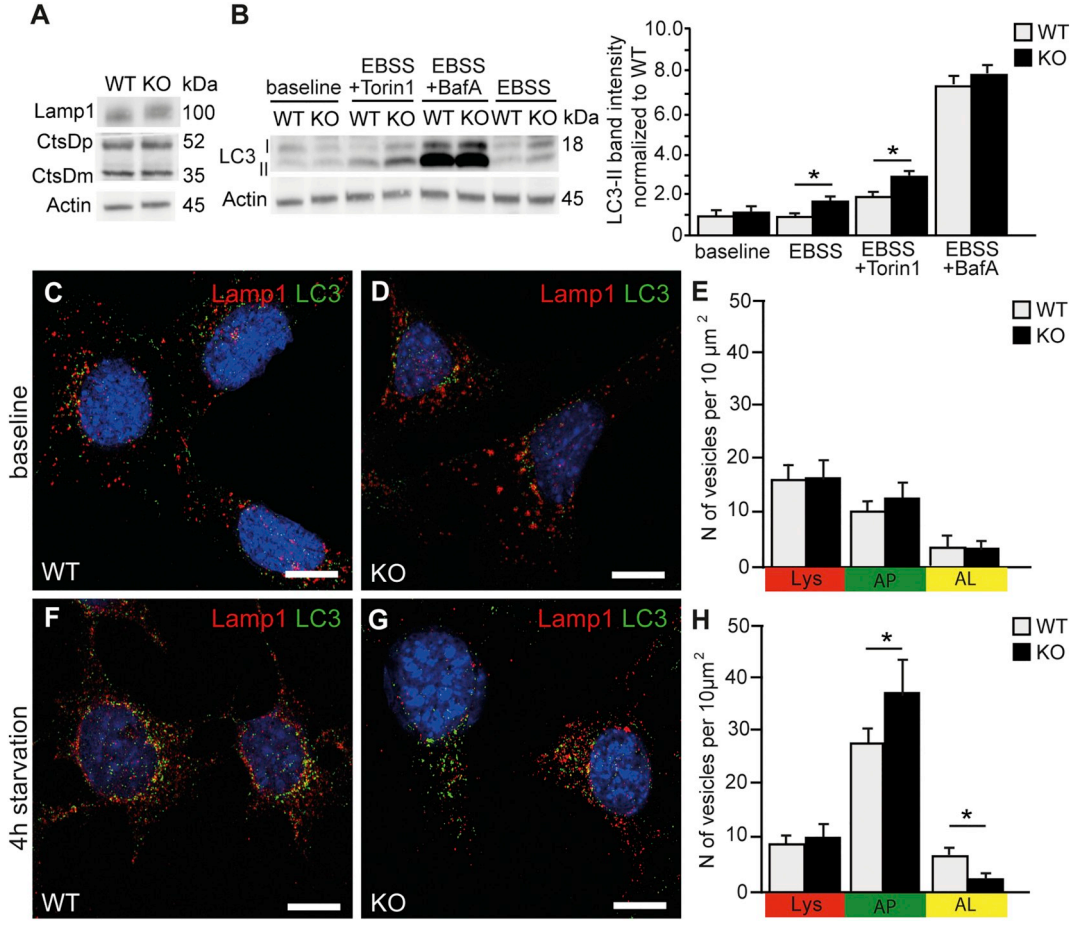

Fig. 5. Impaired autophagy upon disruption of AP5 zeta. (A) Lamp1 protein abundance and the lysosomal processing of the lysosomal protease Cathepsin D precursor (CtsDp) into the mature enzyme (CtsDm) were unchanged in KO MEFs. (B) LC3-I and LC3-II levels at baseline and upon induction of autophagy by EBSS starvation, EBSS starvation plus Torin1, and EBSS after blocking lysosomal degradation by Bafilomycin A (BafA). Actin served as a loading control. Student's *t*-test (three experiments; * $p < 0.05$). (C-H) Quantification of lysosomes (Lys, Lamp1-positive and LC3-negative red puncta), autophagosomes (AP, Lamp1-negative, LC3-positive green puncta), and autolysosomes (AL, Lamp1-positive and LC3-positive yellow puncta) in MEFs at baseline and upon induction of autophagy by starvation supports a defect of autophagic flux. Scale bars: 10 µm. Student's *t*-test (30 cells from three experiments; * $p < 0.05$). Error bars in (B, E, H) represent mean ± SEM. (For interpretation of the references to colour in this figure legend, the reader is referred to the web version of this article.)

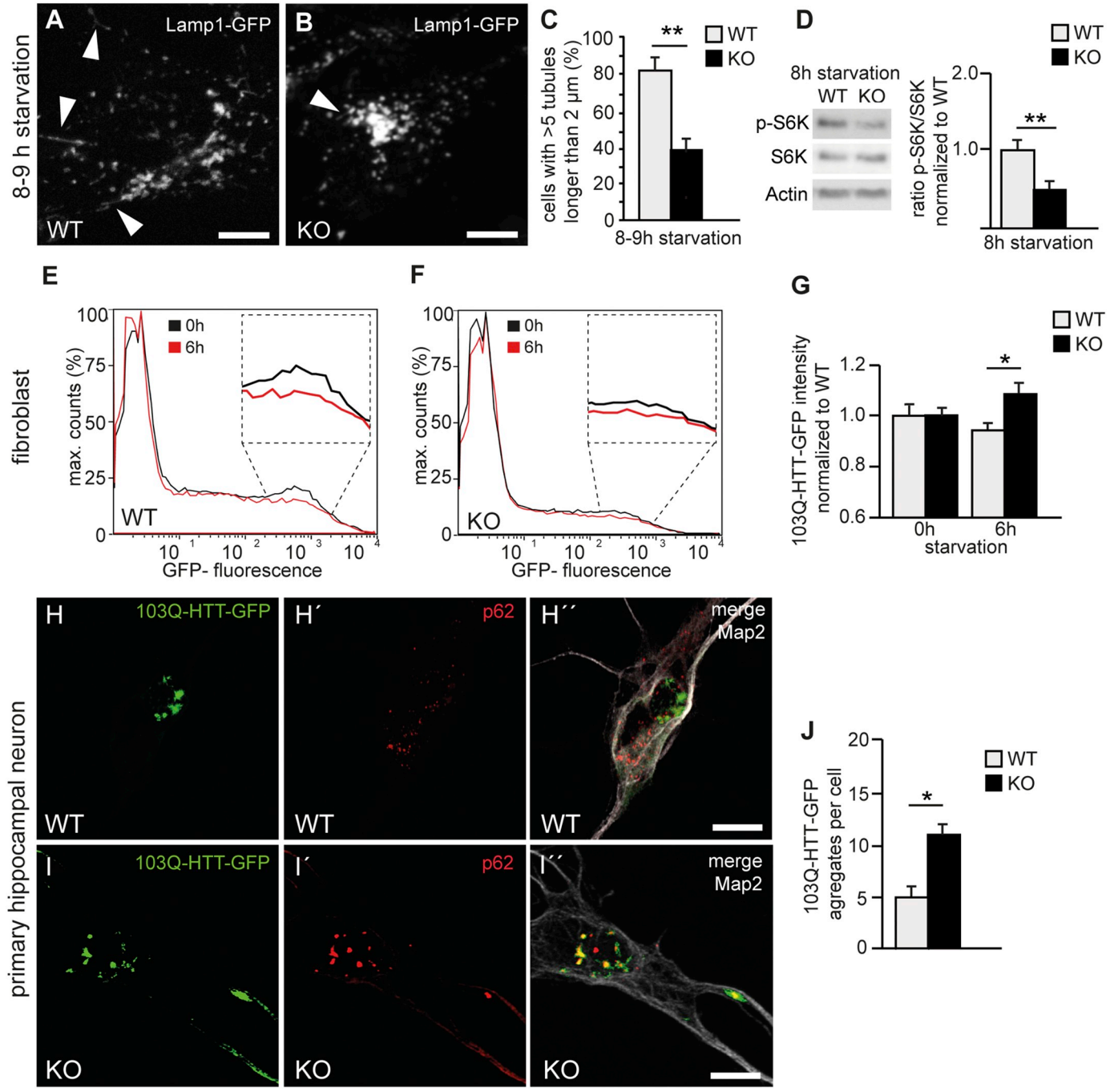

Fig. 6. Impaired autophagic lysosome reformation and increased accumulation of mutant huntingtin aggregates upon disruption of AP5 zeta. (A-C) Autophagic lysosome reformation is impaired in AP5 zeta KO. Cells with more than five Lamp1-positive tubules longer than 2 µm were counted by live cell imaging between eight and nine h of starvation. Student's *t*-test (over 30 cells from three experiments; ** $p < 0.01$). Scale bars: 10 µm. (D) Analysis of the abundance of phosphorylated S6K (p-S6K) compared to total S6K levels in MEFs upon 8 h of starvation. Actin served as a loading control. Student's *t*-test ($n = 3$ experiments; ** $p < .01$). (E-G) Median fluorescence intensity of GFP at 0 h and after 6 h of starvation in MEFs transfected with the aggregation prone 103Q huntingtin (HTT) variant. Student's *t*-test (200,000 cells from three experiments; * $p < 0.05$) (H-J) Number of GFP-positive aggregates per cell in primary hippocampal neurons at day five, 24 h after transfection. Neurons were stained by Map2 (shown in grey). Scale bars: 5 µm. Student's *t*-test (over 10 cells from three experiments; * $p < 0.05$). Error bars in (C, D, G, J) represent mean ± SEM.

in AP5 zeta knockout MEFs may be related to a defect in autophagic lysosome reformation (ALR), occurring upon prolonged starvation (Yu et al., 2010). Therefore, we assessed the extent of protolysosomal tubules forming from autolysosomes by live cell imaging of cells transfected with Lamp1-GFP upon prolonged starvation periods between 8 and 9 h (Fig. 6A, B; Video S1, S2). Strikingly, when compared to WT MEFs, the number of cells with more than five Lamp1-GFP-positive tubules that were longer than 2 µm was significantly reduced in AP5 zeta knockout MEFs (Fig. 6C). Because the recycling of lysosomes from autolysosomes was reported to be regulated by mTOR activity (Yu et al., 2010), we quantified the phosphorylation of its *bona fide* substrate p70S6 Kinase (p-S6K) in MEF lysates under prolonged starvation (eight hours) (Fig. 6D). Interestingly, we detected a significant decrease of S6K phosphorylation in starved AP5 zeta KO MEFs. This result reveals that AP5 zeta should play a role in lysosomal function under challenging conditions, such as starvation. Of note, a decrease of S6K

phosphorylation in cells compromised in ALR has been previously reported (Magalhaes et al., 2016) and is in line with our finding here.

3.6. Impaired degradation of aggregation prone Huntingtin in AP5 zeta knockout MEFs and neurons

To address our assumption that AP5 KO MEFs display a block in the autophagic flux, we transfected wild-type and AP5 zeta knockout MEFs with a GFP-labeled aggregation-prone N-terminal fragment of Huntingtin (103Q-HTT-GFP), which is largely degraded *via* selective autophagy (Ravikumar et al., 2004), and measured GFP fluorescence intensity by flow cytometry over time as an indicator for the autophagic flux. Upon starvation of AP5 KO MEFs a significant increase in GFP fluorescence was found which suggests that less 103Q-HTT-GFP was degraded under these conditions (Fig. 6E-G). This finding goes in line with our previously described results. We also addressed this question in primary neurons derived from WT and AP5 zeta KO mice. Confirming a defect in the degradative capacity of AP5 zeta KO neurons, the number of 103Q-HTT-GFP and p62-positive aggregates per neuron was significantly increased at day five *in vitro* (Fig. 6H-J).

Taken together, we provide evidence that AP5 should be a critical factor for lysosomal function and autophagic degradation in stress conditions.

3.7. Accumulation of autophagic material in vivo in AP5 zeta knockout mice

We asked whether the results obtained in MEFs and cultured neurons also apply *in vivo*. As in cultured MEFs overall Lamp1 abundance was not changed in brain lysates of 20-month-old mice and the lysosomal processing of cathepsin D was intact (Fig. 7A-C). Moreover, levels of mTOR, the key regulator of autophagy, and Beclin 1, which is involved in the control of autophagosome formation (Wirawan et al., 2012), did not differ between genotypes. Notably, however, levels of the autophagic cargo receptor p62 (Danieli and Martens, 2018), which recognizes toxic cellular waste and is then scavenged by autophagy, were significantly increased in Triton X-100 insoluble brain fractions of 20-month-old knockout mice. Moreover, the p62 signal localized to autofluorescent deposits in brain sections of 20-month-old knockout mice (Fig. 7D-D″), which also labeled for Lamp1 (Fig. 7E-E″).

In analogy to our experiments with MEFs we also quantified lysosomes, autophagosomes, and autolysosomes in Purkinje cell bodies in brain sections of two-month-old mice, a time-point before we detected autofluorescent material. While Lamp1-positive but p62-negative lysosomes (red puncta) did not differ between genotypes, p62-positive but Lamp1-negative autophagosomes (green puncta) and Lamp1- and p62-positive autolysosomes (yellow puncta) were significantly increased (Fig. 7F-H).

Thus, our *in vivo* data strongly support our previous results achieved *in vitro* (Fig. 5), demonstrating an accumulation of autophagic vesicles through a block in the autophagic flux in neurons of AP5 zeta KO mice (Fig. 6).

4. Discussion

4.1. AP5 zeta knockout mice are a valid model for SPG48

SPG11, SPG15, and SPG48 are closely related disorders with overlapping symptoms such as intellectual disability, sensorimotor neuropathy, hereditary spastic paraplegia, ataxia, and Parkinsonism. The majority of SPG48 genotypes, however, manifest with a later age at onset and intellectual disability is less frequent and rather mild compared with SPG11 and SPG15 patients (Pensato et al., 2014; Schlipf et al., 2014; Hirst et al., 2016), which often present with learning difficulties in childhood as the first symptom before the spasticity manifests during the second or third decades. In agreement with the clinical presentation, AP5 zeta knockout mice are less severely affected than the mouse models for SPG11 and SPG15 (Khundadze et al., 2013; Varga et al., 2015) and do not develop cognitive deficits up to six months of age. While Spatacsin and Spastizin knockout mice are almost paralyzed at 20 months of age and display severe brain atrophy with neuronal loss, this does not apply to AP5 zeta knockout mice. Nevertheless, a loss of large diameter axons in the lumbar corticospinal tract as a typical hallmark of HSP (Fink, 2014) was clearly observed.

4.2. Accumulation of lysosome-related material in AP5 zeta knockout mice

Axonal loss was further associated with the occurrence of axonal swellings, which have also been reported in other mouse models of HSP such as *e.g.* SPG2 (Edgar et al., 2004), SPG4 (Tarrade et al., 2006), SPG7 (Ferreirinha et al., 2004) and, more recently, SPG51 (De Pace et al., 2018). Notably, the latter is caused by mutations in the gene encoding the epsilon subunit of the adaptor protein 4 complex (AP4) (Abou Jamra et al., 2011). Similar to results obtained for AP4 epsilon knockout mice (De Pace et al., 2018), axonal swellings are also Lamp1-positive upon disruption of AP5 zeta. From our ultrastructural analysis these swellings correspond with clusters of organelles and vesicles resembling lysosomes, autolysosomes or autophagic vesicles. Focal axonal swellings are encountered in several neurodegenerative disorders, including multiple sclerosis, motor neuron disease, spastic paraplegia, and Alzheimer's disease. Although there is growing evidence that deficits in axonal transport such as observed in SPG10 (Blackstone et al., 2011) may contribute to axonal swellings, it is yet unclear whether this also applies to AP5 knockout mice.

Lamp1-positive material also accumulates in Purkinje cell bodies of AP5 zeta knockout mice and is characterized by a strong autofluorescence and likely correlates with clusters of electron dense material of irregular shape, which are bordered by membranes, resembling residual bodies filled with indigestible materials, which are considered as nondegradable intralysosomal material (Terman and Brunk, 2004). In any case, it is conceivable that at some point these intracellular deposits impair intracellular transport and thus contribute to the cellular pathology.

4.3. Disruption of AP5 zeta results in a fragmentation of the Golgi apparatus

Previous findings suggested that AP5 is involved as a backup system for the retrieval from late endosomes to the *trans*Golgi network (TGN) based on subcellular fractionation profiling and quantitative mass spectrometry, which identified some Golgi proteins to be mis-localized (Hirst et al., 2018). Since we considered that AP5 might play a role for lysosome homeostasis, we chose a similar approach and compared the proteome of lysosomes from wild-type and knockout MEFs. Similar to the previous report (Hirst et al., 2018), we also found a number of usually Golgi resident proteins including Glg1 to be increased in the lysosomal fraction, but no obviously meaningful changes of lysosomal proteins. While the function of Glg1 is still elusive, our findings are in agreement with the idea that AP5 may play a role for the retrieval of proteins from late endosomes to the TGN, which is also supported by our data that the transport of M6PR towards the TGN was impaired in knockout MEFs. However, we also noted a robust decrease of TGN38 signals in knockout MEFs and a smaller and more vesiculated Golgi apparatus by ultrastructural analysis. Notably, similar alterations were found upon disruption of the Golgi protein GM130, which also develop Purkinje cell pathologies (Liu et al., 2017). Such alterations of the Golgi are a quite frequent finding in neurodegenerative disorders including Alzheimer's disease, Parkinson's disease, amyotrophic lateral sclerosis (ALS) and spinocerebellar ataxia (Gonatas et al., 1992; Stieber et al., 1996; Mizuno et al., 2001; Huynh et al., 2003; Nakagomi et al., 2008). Still it is tempting to speculate that the structural changes might be a consequence of a defect in the retrieval of Golgi proteins from late

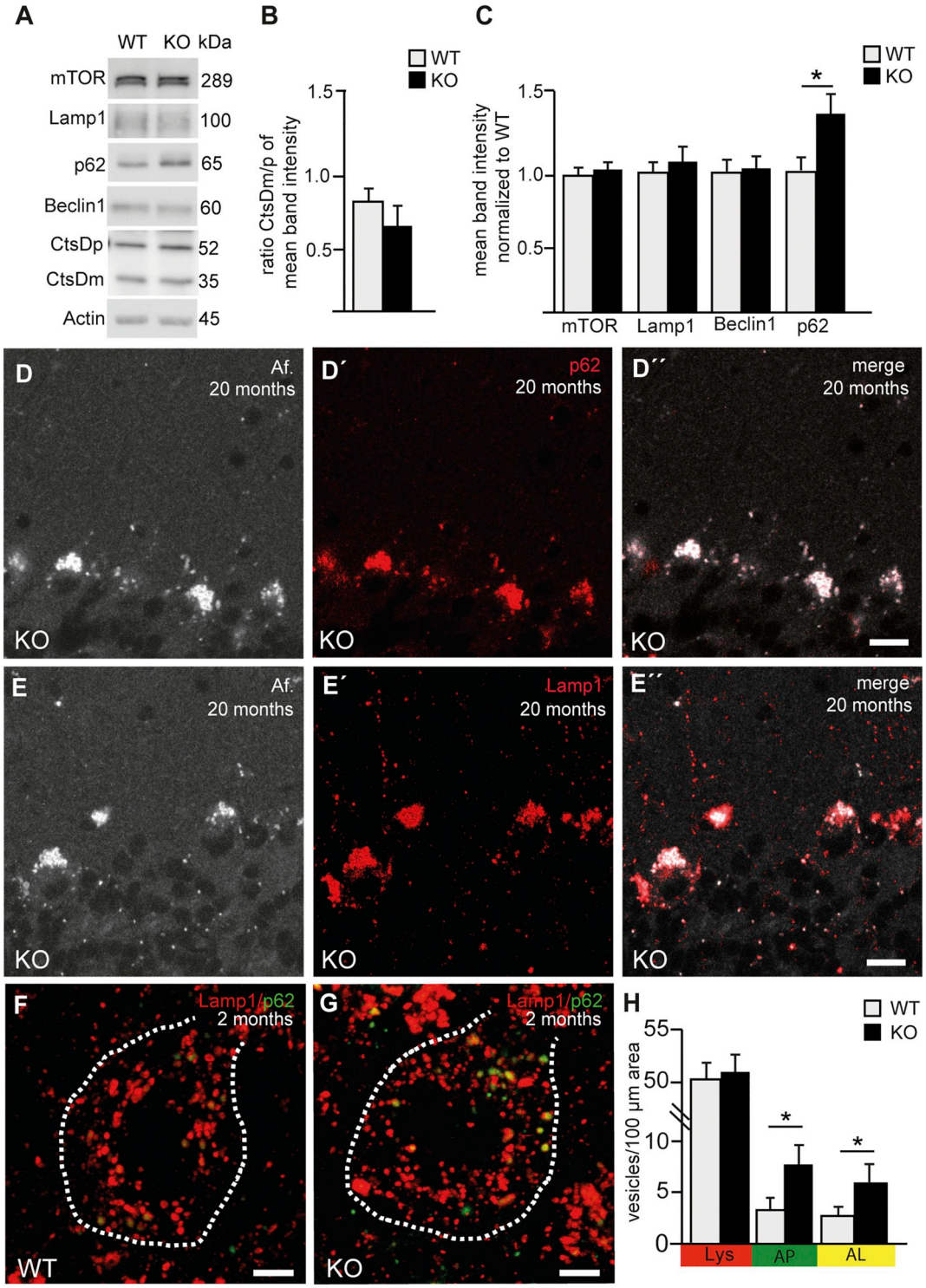

Fig. 7. Impaired autophagy in AP5 zeta knockout mice. (A-C) mTOR, Lamp1, Beclin1 abundance and lysosomal processing of the lysosomal protease Cathepsin D precursor (CtsDp) into the mature enzyme (CtsDm) are not changed in brain lysates from 20-month-old knockout mice, while p62 levels (Triton X insoluble fraction) are increased. Actin served as a loading control. Student's *t*-test (three mice per genotype; * $p < 0.05$). (D-E″) Autofluorescent deposits in AP5 zeta knockout brains are positive for both Lamp1 and p62. Scale bars: 10 µm. Af: Autofluorescence. (F-H) Quantification of lysosomes (Lys, Lamp1-positive and p62-negative red puncta), autophagosomes (AP, Lamp1-negative and p62-positive green puncta), and autolysosomes (AL, Lamp1-positive and p62-positive yellow puncta) in Purkinje cells in brain sections of three-month-old mice before accumulation of autofluorescent material are in agreement with a defect in autophagy. Scale bars: 5 µm. Student's *t*-test (over 30 cells from three mice per genotype; * $p < 0.05$). Error bars in (B, C, H) represent mean ± SEM. (For interpretation of the references to colour in this figure legend, the reader is referred to the web version of this article.)

endosomes. Our data that changes in Golgi proteins in immunofluorescence stainings were only observed at 20 months, but not at two months of age, rather argue for a minor role of AP5 for the retrieval from late endosomes to the TGN.

4.4. Dysfunctional autophagy upon disruption of AP5 zeta

As a first hint that autophagy under stressed conditions is compromised upon disruption of AP5 zeta, the number of autophagosomes was increased in starved knockout MEFs while the number of lysosomes was reduced. Increased autophagosome numbers were also observed in fibroblasts of SPG15 patients as well as in Spastizin knockdown studies in primary mouse neurons (Vantaggiato et al., 2013; Vantaggiato et al., 2018) and in HeLa cells upon knockdown of either Spastizin or Spatacsin (Chang et al., 2014). As also shown for Spastizin and Spatacsin (Chang et al., 2014), the extent of protolysosomal tubules forming from autolysosomes upon prolonged starvation periods was reduced in the absence of AP5 zeta. The defect in ALR in AP5 zeta deficient cells does not occur as a secondary effect of reduced Spastizin and Spatacsin protein abundance, but we cannot rule out that it is caused by a wrong localization of Spastizin and Spatacsin upon disruption of AP5 zeta. Notably, a trend towards enlargement of autolysosomes was reported after knock-down of the beta subunit of AP5, but tubulation itself was not analyzed (Chang et al., 2014). Further supporting a defect in ALR, the abundance of p-S6K was reduced in AP5 knockout MEFs and did not recover upon prolonged starvation, similar to cells lacking functional glucocerebrosidase, in which autophagic lysosome reformation is impaired (Magalhaes et al., 2016). Whether blocked autophagy in AP5 zeta knockout MEFs is a consequence of defective autophagic lysosome reformation (ALR) or *vice versa* we cannot answer for the time being.

Because lysosomes are organelles critical for terminating autophagy *via* their fusion with mature autophagosomes to generate autolysosomes that degrade autophagic materials, impairment of autophagic lysosome reformation will have consequences on the clearance of cellular components *via* autophagy. This includes the degradation of abnormal proteins, which is also largely mediated *via* autophagy (Hara et al., 2006; Komatsu et al., 2006; Mizushima, 2007) and a common cause of neuronal degeneration (Williams et al., 2006; Martini-Stoica et al., 2016). Indeed, the degradation of an aggregation prone GFP-tagged Huntingtin variant was impaired in both MEFs and primary neurons of AP5 zeta knockout mice. In the long term, defective autophagy will thus lead to the accumulation of undegraded material as observed in aged knockout mice.

In summary, we show that disruption of AP5 results in defective autophagy upon challenged conditions, which reduces the degradative capacity and causes the accumulation of autophagic cargo and possibly toxic proteins. This scenario may be aggravated by alterations of the Golgi apparatus. Future studies will hopefully help to resolve how AP5, Spastizin and Spatacsin interact to regulate autophagy and the recycling of lysosomes from autolysosomes.

Supplementary data to this article can be found online at https://doi.org/10.1016/j.nbd.2019.03.026.

Competing interests

The authors report no competing interests.

Funding

This study was funded by grants of the IZKF to MK (J47) and DFG to CAH (HU 800/10-1 and HU 800/13-1 (FOR 2625). DW, TS, JK, MD, TP-C, CAH are co-funded by the DFG FOR2625.

Acknowledgements

We thank Dr. Christoph Kaether (Leibniz Institute on Aging – Fritz Lipmann Institute, Jena) for reagents and helpful discussions, Katrin Schorr (Institute of Human Genetics, University Hospital Jena) for blastocyst injection and Annett Bueschel (Institute of Clinical Chemistry and Lab Diagnostics, University Hospital Jena) for preparation of primary neuron cultures.

References

Abou Jamra, R., Philippe, O., Raas-Rothschild, A., Eck, S.H., Graf, E., Buchert, R., et al., 2011. Adaptor protein complex 4 deficiency causes severe autosomal-recessive intellectual disability, progressive spastic paraplegia, shy character, and short stature. Am. J. Hum. Genet. 88 (6), 788–795.

Ashburner, M., Ball, C.A., Blake, J.A., Botstein, D., Butler, H., Cherry, J.M., et al., 2000. Gene ontology: tool for the unification of biology. The Gene Ontology Consortium. Nat. Genet. 25 (1), 25–29.

Beetz, C., Koch, N., Khundadze, M., Zimmer, G., Nietzsche, S., Hertel, N., et al., 2013. A spastic paraplegia mouse model reveals REEP1-dependent ER shaping. J. Clin. Invest. 123 (10), 4273–4282.

Blackstone, C., 2018. Hereditary spastic paraplegia. Handb. Clin. Neurol. 148, 633–652.

Blackstone, C., Kane, C.J., Reid, E., 2011. Hereditary spastic paraplegias: membrane traffic and the motor pathway. Nat. Rev. Neurosci. 12, 31–42.

Chang, J., Lee, S., Blackstone, C., 2014. Spastic paraplegia proteins spastizin and spatacsin mediate autophagic lysosome reformation. J. Clin. Invest. 124 (12), 5249–5262.

Danieli, A., Martens, S., 2018. p62-mediated phase separation at the intersection of the ubiquitin-proteasome system and autophagy. J. Cell Sci. 131 (19).

De Pace, R., Skirzewski, M., Damme, M., Mattera, R., Mercurio, J., Foster, A.M., et al., 2018. Altered distribution of ATG9A and accumulation of axonal aggregates in neurons from a mouse model of AP-4 deficiency syndrome. PLoS Genet. 14 (4), e1007363.

Denton, K., Mou, Y., Xu, C.C., Shah, D., Chang, J., Blackstone, C., et al., 2018. Impaired mitochondrial dynamics underlie axonal defects in hereditary spastic paraplegias. Hum. Mol. Genet. 27 (14), 2517–2530.

Edgar, J.M., McLaughlin, M., Barrie, J.A., McCulloch, M.C., Garbern, J., Griffiths, I.R., 2004. Age-related axonal and myelin changes in the rumpshaker mutation of the Plp gene. Acta Neuropathol. 107 (4), 331–335.

Falcon-Perez, J.M., Nazarian, R., Sabatti, C., Dell'Angelica, E.C., 2005. Distribution and dynamics of Lamp1-containing endocytic organelles in fibroblasts deficient in BLOC-3. J. Cell Sci. 118 (Pt 22), 5243–5255.

Ferreirinha, F., Quattrini, A., Pirozzi, M., Valsecchi, V., Dina, G., Broccoli, V., et al., 2004. Axonal degeneration in paraplegin-deficient mice is associated with abnormal mitochondria and impairment of axonal transport. J. Clin. Invest. 113 (2), 231–242.

Fink, J.K., 2014. Hereditary spastic paraplegia: clinical principles and genetic advances. Semin. Neurol. 34 (3), 293–305.

Gonatas, N.K., Stieber, A., Mourelatos, Z., Chen, Y., Gonatas, J.O., Appel, S.H., et al., 1992. Fragmentation of the Golgi apparatus of motor neurons in amyotrophic lateral sclerosis. Am. J. Pathol. 140 (3), 731–737.

Hara, T., Nakamura, K., Matsui, M., Yamamoto, A., Nakahara, Y., Suzuki-Migishima, R., et al., 2006. Suppression of basal autophagy in neural cells causes neurodegenerative disease in mice. Nature 441 (7095), 885–889.

Hirst, J., Barlow, L.D., Francisco, G.C., Sahlender, D.A., Seaman, M.N., Dacks, J.B., et al., 2011. The fifth adaptor protein complex. PLoS Biol. 9 (10), e1001170.

Hirst, J., Borner, G.H., Edgar, J., Hein, M.Y., Mann, M., Buchholz, F., et al., 2013. Interaction between AP-5 and the hereditary spastic paraplegia proteins SPG11 and SPG15. Mol. Biol. Cell 24 (16), 2558–2569.

Hirst, J., Edgar, J.R., Esteves, T., Darios, F., Madeo, M., Chang, J., et al., 2015. Loss of AP-5 results in accumulation of aberrant endolysosomes: defining a new type of lysosomal storage disease. Hum. Mol. Genet. 24 (17), 4984–4996.

Hirst, J., Madeo, M., Smets, K., Edgar, J.R., Schols, L., Li, J., et al., 2016. Complicated spastic paraplegia in patients with AP5Z1 mutations (SPG48). Neurol. Genet. 2 (5), e98.

Hirst, J., Itzhak, D.N., Antrobus, R., Borner, G.H.H., Robinson, M.S., 2018. Role of the AP-5 adaptor protein complex in late endosome-to-Golgi retrieval. PLoS Biol. 16 (1), e2004411.

Huynh, D.P., Yang, H.T., Vakharia, H., Nguyen, D., Pulst, S.M., 2003. Expansion of the polyQ repeat in ataxin-2 alters its Golgi localization, disrupts the Golgi complex and causes cell death. Hum. Mol. Genet. 12 (13), 1485–1496.

Khundadze, M., Kollmann, K., Koch, N., Biskup, C., Nietzsche, S., Zimmer, G., et al., 2013. A hereditary spastic paraplegia mouse model supports a role of ZFYVE26/SPASTIZIN for the endolysosomal system. PLoS Genet. 9 (12), e1003988.

Komatsu, M., Waguri, S., Chiba, T., Murata, S., Iwata, J., Tanida, I., et al., 2006. Loss of autophagy in the central nervous system causes neurodegeneration in mice. Nature 441 (7095), 880–884.

Liu, C., Mei, M., Li, Q., Roboti, P., Pang, Q., Ying, Z., et al., 2017. Loss of the golgin GM130 causes Golgi disruption, Purkinje neuron loss, and ataxia in mice. Proc. Natl. Acad. Sci. U. S. A. 114 (2), 346–351.

Magalhaes, J., Gegg, M.E., Migdalska-Richards, A., Doherty, M.K., Whitfield, P.D., Schapira, A.H., 2016. Autophagic lysosome reformation dysfunction in glucocerebrosidase deficient cells: relevance to Parkinson disease. Hum. Mol. Genet. 25 (16), 3432–3445.

Martini-Stoica, H., Xu, Y., Ballabio, A., Zheng, H., 2016. The autophagy-Lysosomal pathway in Neurodegeneration: a TFEB perspective. Trends Neurosci. 39 (4), 221–234.

Meriin, A.B., Zhang, X., He, X., Newnam, G.P., Chernoff, Y.O., Sherman, M.Y., 2002. Huntington toxicity in yeast model depends on polyglutamine aggregation mediated by a prion-like protein Rnq1. J. Cell Biol. 157 (6), 997–1004.
Mizuno, Y., Hattori, N., Kitada, T., Matsumine, H., Mori, H., Shimura, H., et al., 2001. Familial Parkinson's disease. Alpha-synuclein and parkin. Adv. Neurol. 86, 13–21.
Mizushima, N., 2007. Autophagy: process and function. Genes Dev. 21 (22), 2861–2873.
Nakagomi, S., Barsoum, M.J., Bossy-Wetzel, E., Sutterlin, C., Malhotra, V., Lipton, S.A., 2008. A Golgi fragmentation pathway in neurodegeneration. Neurobiol. Dis. 29 (2), 221–231.
Pensato, V., Castellotti, B., Gellera, C., Pareyson, D., Ciano, C., Nanetti, L., et al., 2014. Overlapping phenotypes in complex spastic paraplegias SPG11, SPG15, SPG35 and SPG48. Brain 137 (Pt 7), 1907–1920.
Ravikumar, B., Vacher, C., Berger, Z., Davies, J.E., Luo, S., Oroz, L.G., et al., 2004. Inhibition of mTOR induces autophagy and reduces toxicity of polyglutamine expansions in fly and mouse models of Huntington disease. Nat. Genet. 36 (6), 585–595.
Sagona, A.P., Nezis, I.P., Pedersen, N.M., Liestol, K., Poulton, J., Rusten, T.E., et al., 2010. PtdIns(3)P controls cytokinesis through KIF13A-mediated recruitment of FYVE-CENT to the midbody. Nat. Cell Biol. 12 (4), 362–371.
Schlipf, N.A., Schule, R., Klimpe, S., Karle, K.N., Synofzik, M., Wolf, J., et al., 2014. AP5Z1/SPG48 frequency in autosomal recessive and sporadic spastic paraplegia. Mol. Genet. Genomic Med. 2 (5), 379–382.
Sinning, A., Liebmann, L., Kougioumtzes, A., Westermann, M., Bruehl, C., Hubner, C.A., 2011. Synaptic glutamate release is modulated by the Na^+-driven Cl^-/HCO_3^- exchanger Slc4a8. J. Neurosci. 31 (20), 7300–7311.
Skarnes, W.C., Rosen, B., West, A.P., Koutsourakis, M., Bushell, W., Iyer, V., et al., 2011. A conditional knockout resource for the genome-wide study of mouse gene function. Nature 474 (7351), 337–342.
Slabicki, M., Theis, M., Krastev, D.B., Samsonov, S., Mundwiller, E., Junqueira, M., et al., 2010. A genome-scale DNA repair RNAi screen identifies SPG48 as a novel gene associated with hereditary spastic paraplegia. PLoS Biol. 8 (6), e1000408.
Stieber, A., Mourelatos, Z., Gonatas, N.K., 1996. In Alzheimer's disease the Golgi apparatus of a population of neurons without neurofibrillary tangles is fragmented and atrophic. Am. J. Pathol. 148 (2), 415–426.
Tarrade, A., Fassier, C., Courageot, S., Charvin, D., Vitte, J., Peris, L., et al., 2006. A mutation of spastin is responsible for swellings and impairment of transport in a region of axon characterized by changes in microtubule composition. Hum. Mol. Genet. 15 (24), 3544–3558.
Terman, A., Brunk, U.T., 2004. Lipofuscin. Int. J. Biochem. Cell Biol. 36 (8), 1400–1404.
The Gene Ontology C, 2017. Expansion of the gene ontology knowledgebase and resources. Nucleic Acids Res. 45 (D1), D331–D338.
Thelen, M., Winter, D., Braulke, T., Gieselmann, V., 2017. SILAC-based comparative proteomic analysis of lysosomes from mammalian cells using LC-MS/MS. Methods Mol. Biol. 1594, 1–18.
Vantaggiato, C., Crimella, C., Airoldi, G., Polishchuk, R., Bonato, S., Brighina, E., et al., 2013. Defective autophagy in spastizin mutated patients with hereditary spastic paraparesis type 15. Brain 136, 3119–3139 Pt 10.
Vantaggiato, C., Clementi, E., Bassi, M.T., 2014. ZFYVE26/SPASTIZIN: a close link between complicated hereditary spastic paraparesis and autophagy. Autophagy 10 (2), 374–375.
Vantaggiato, C., Panzeri, E., Castelli, M., Citterio, A., Arnoldi, A., Santorelli, F.M., et al., 2018. ZFYVE26/SPASTIZIN and SPG11/SPATACSIN mutations in hereditary spastic paraplegia types AR-SPG15 and AR-SPG11 have different effects on autophagy and endocytosis. Autophagy 1–24.
Varga, R.E., Khundadze, M., Damme, M., Nietzsche, S., Hoffmann, B., Stauber, T., et al., 2015. In vivo evidence for lysosome depletion and impaired Autophagic clearance in hereditary spastic paraplegia type SPG11. PLoS Genet. 11 (8), e1005454.
Weinert, S., Jabs, S., Supanchart, C., Schweizer, M., Gimber, N., Richter, M., et al., 2010. Lysosomal pathology and osteopetrosis upon loss of H^+-driven lysosomal Cl^- accumulation. Science 328 (5984), 1401–1403.
Williams, A., Jahreiss, L., Sarkar, S., Saiki, S., Menzies, F.M., Ravikumar, B., et al., 2006. Aggregate-prone proteins are cleared from the cytosol by autophagy: therapeutic implications. Curr. Top. Dev. Biol. 76, 89–101.
Wirawan, E., Lippens, S., Vanden Berghe, T., Romagnoli, A., Fimia, G.M., Piacentini, M., et al., 2012. Beclin1: a role in membrane dynamics and beyond. Autophagy 8 (1), 6–17.
Yu, L., McPhee, C.K., Zheng, L., Mardones, G.A., Rong, Y., Peng, J., et al., 2010. Termination of autophagy and reformation of lysosomes regulated by mTOR. Nature 465 (7300), 942–946.